coatings

MDPI

Article

Synergistic Effect of Mica, Glass Frit, and Melamine Cyanurate for Improving Fire Resistance of Styrene-Butadiene Rubber Composites Destined for Ceramizable Coatings

Mateusz Imiela [1], Rafał Anyszka [1,2,*], Dariusz M. Bieliński [1], Magdalena Lipińska [1], Przemysław Rybiński [3] and Bartłomiej Syrek [3]

1 Institute of Polymer & Dye Technology, Faculty of Chemistry, Lodz University of Technology, Stefanowskiego 12/16, 90-924 Łódź, Poland; mateusz.imiela@edu.p.lodz.pl (M.I.); dariusz.bielinski@p.lodz.pl (D.M.B.); magdalena.lipinska@p.lodz.pl (M.L.)

2 Department of Mechanics of Solids, Surfaces & Systems (MS3), Faculty of Engineering Technology, Chair of Elastomer Technology & Engineering, University of Twente, 7500 AE Enschede, The Netherlands

3 Management of Environment Protection and Modeling, The Jan Kochanowski University, Żeromskiego 5, Kielce 25-369, Poland; przemyslaw.rybinski@ujk.edu.pl (P.R.); barlomiej.syrek@ujk.edu.pl (B.S.)

* Correspondence: rafal.anyszka@p.lodz.pl or r.p.anyszka@utwente.nl; Tel.: +315-3489-1407

Received: 21 December 2018; Accepted: 27 February 2019; Published: 5 March 2019

Abstract: Synergistic effects of different fillers are widely utilized in polymer technology. The combination of various types of fillers is used to improve various properties of polymer composites. In this paper, a synergistic effect of flame retardants was tested to improve the performance of ceramizable composites. The composites were based of styrene-butadiene rubber (SBR) used as polymer matrix. Three different types of flame retardants were tested for synergistic effect: Mica (phlogopite) high aspect-ratio platelets, along with low softening point temperature glass frit (featuring ceramization effect), and melamine cyanurate, a commonly used flame retardant promoting carbonaceous char. In order to characterize the properties of the composites, combustibility, thermal stability, viscoelastic properties, micromorphology, and mechanical properties were tested before and after ceramization. The results obtained show that the synergistic effect of ceramization promoting fillers and melamine cyanurate was especially visible with respect to the flame retardant properties resulting in a significant improvement of fire resistance of the composites.

Keywords: composite; ceramization; ceramification; styrene-butadiene rubber; melamine cyanurate; mica; flame retardancy; coating; glass frit

1. Introduction

Ceramizable (ceramifiable) polymer composites were originally designed and developed for cable coatings ensuring integration of an electric installation in case of a fire-hazard [1–3]. Such approach resulted in a significant enhancement in evacuation techniques and fire-fighting systems. For example, allowing for the development of fireproof elevators ensuring effective evacuation possibilities, especially for disabled or elderly people [4]. Moreover, in recent years the area of ceramizable composites utilization expanded covering the fireproof window sealing system [5], coatings for steel construction elements [6], and innovative ablative materials for spacecraft applications [7], starting to compete with much more popular now intumescent coatings [8].

Ceramizable polymer composites are a type of smart materials changing their structure and properties when exposed to fire and elevated temperature. They exhibit high elasticity and easy

processing before ceramization and transform into a continuous and stiff ceramic structure after ceramization. From a morphological point of view they are dispersion composites consisting of polymer matrix and a mix of dispersed fillers that initiate the ceramization process. The polymer matrix burns and decomposes at elevated temperatures, while the fillers interact forming a continuous ceramic structure.

There are several mechanisms of ceramization: (1) addition of a low softening point temperature glass frit that acts as a binding agent for other thermally stable fillers [9–11]; (2) sintering of filler particles accompanied by silicone rubber matrix covalently bonded to their surface [12]; (3) in-situ formation of calcium silicates from calcium-based fillers and the silica formed after silicone matrix burning [1]; (4) silicon oxycarbide phase formation from cross-linking of silicone rubber adsorbed on nano-filler surface or catalyzed by platinum compounds [13]; (5) in-situ ceramic structure formation from reactions between the products of thermal decomposition of silicone rubber, ammonium polyphosphate, aluminum hydroxide, and mica [14]; and (6) controlled arrangement of mineral fillers inside the polymer matrix [15]. A specific type of secondary filler may be used in order to improve the ceramic structure's properties, for example, triggering the formation of a nano-porous phase [16] or enhancing its compression strength [17].

Silicone rubber was originally chosen as a ceramizable composites matrix because amorphous silica is the product of its burning, which improves the properties of the ceramic phase. However, silicone rubber exhibits also some limitations like relatively low mechanical properties, high price, and low filler loading. Therefore, alternative polymer matrices are tested for ceramizable composite applications, such as: acrylonitrile-butadiene rubber (NBR) [18], ethylene-propylene-diene rubber (EPDM) [19–21], poly(vinyl acetate) [22], polyurethane [23], polyester [24], polyethylene [25], and boron phenolic resin [26–28]. However, their applicability as ceramizable composites remains limited. The most promising replacement for silicone rubber nowadays seems to be the poly(ethylene-co-vinyl acetate) copolymer (EVA), ensuring good mechanical properties both before and after ceramization [29–32]. The positive effects of EVA application as a matrix for ceramizable composites resulted also in using it as a blend with silicone rubber [33]. However, the use of silicone rubber alone is still very prospective [34,35]. In our previous work we proved that the application of styrene-butadiene rubber (SBR) as a polymer matrix for ceramizable composites is also very promising [36]. Based on the available literature [37–39], one can state that thermal stability of SBR is comparable to that of silicone rubber [40,41]. Moreover, in the presence of oxygen, SBR degrades with two-stage kinetics [38], first occurring in the temperature range of 390–520 °C and subsequently between 620 and 720 °C. The first stage most probably corresponds to the thermal degradation of linear rubber macromolecules and the simultaneous cross-linking (maybe even carbonization) leading to the formation of a thermally stable residue that decomposes thermooxidatively in the second stage. The highly cross-linked structure formed during thermal degradation plays most likely a significant role in maintaining a coherent, self-supporting structure of the ceramizable composites in the temperature range where the elastic SBR matrix is gone but the new ceramic structure is not fully formed yet [36]. For this reason, SBR rubbers emerge as very prospective matrix materials for ceramizable composites.

In the current work we test the effect of the melamine cyanurate (MCA) addition on the properties of SBR-based ceramizable composites. We aimed to investigate the potential synergistic effects of MCA, mica platelets, and glass frit promoting ceramization on the flame retardancy performance of composites. MCA has proven itself an effective rubber flame retardant [42,43], and has been already successfully applied for enhancing flame retardancy of EVA-based ceramizable composites [31]. Furthermore, the combination of glass frit and mica for SBR-based composites showed an outstanding ceramization performance [36].

2. Materials and Methods

2.1. Materials

Styrene-butadiene rubber (trade name KER 1500) was used as the polymer matrix. It was synthesized by the emulsion method (e-SBR) and purchased from Synthos S.A., Oswiecim, Poland. The rubber contains 22–25 wt.% of bonded styrene, 5.0–7.5 wt.% of organic acids, max. 0.7 wt.% of volatile matters, max. 0.4 wt.% of soaps and max., and 0.4 wt.% of total ash. Its viscosity (ML 1 + 4; 100 °C) ranges 45–55 ML. The ceramization promoting glass frit "A 4015" of chemical composition (wt.%): $4Li_2O$–$16Na_2O$–$37B_2O_3$–$43SiO_2$ and softening point temperature of 540 °C originated from Reimbold & Strick GmbH, Cologne, Germany. Mica (phlogopite) "PW30" (specific surface area of 2.8 m^2/g), produced by LKAB Minerals GmbH (Lulea, Sweden) was used as a temperature resistant mineral filler. Melamine cyanurate (MCA), trade name Budit 315, originated from Brenntag Polska, Kędzierzyn-Koźle, Poland. The cross-linking system–sulphur, accelerator (N-Cyclohexyl-2-benzothiazole sulfenamide (CBS)), activators (stearic acid, ZnO), and antioxidant (2,2,4-trimethyl-1,2-dihydroquinoline (TMQ)), were purchased from Torimex-Chemicals Ltd., Sp. z o. o., Konstantynów Łódzki, Poland.

2.2. Preparation of the Samples

The composite mixes (Table 1) were prepared using a laboratory two-roll mill (the rolls length 200 mm; diameter 150 mm; Bridge, UK), working with the rotation speed of the slower roll of 18 rpm (revolutions per minute) and the faster roll of 20 rpm (friction: 1.1). Kinetics of vulcanization of the composite mixes were tested by means of rheometer Alpha Technologies MDR2000 according to ISO 37:1994 standard [44] (temperature: 160 °C, frequency: 1.667 Hz, strain: 0.5°). According to the results obtained) the samples were shaped and vulcanized in steel molds by a laboratory press at 160 °C and under 10 MPa of pressure.

Table 1. Composition (in phr—parts per hundred parts of rubber) of the ceramizable composites mixes.

Ingredients	Composition of the Samples (phr)					
	Cyan_1	Cyan_2	Cyan_3	Cyan_4	Cyan_5	Cyan_6
SBR	100	100	100	100	100	100
Mica	–	200	–	200	200	175
Glass frit	–	–	100	100	100	75
MCA	50	50	50	25	50	100
Curatives	10	10	10	10	10	10

2.3. Techniques

Viscoelastic properties measurements were made by MonTech RPA 3000 rheometer according to the ASTM D6204 standard [45], Part A for low strain and Part B for high strain. The measurements were made at 100 °C temperature and growing frequencies: 0.1, 0.2, 0.4, 0.6, 0.8, 1, 2, 5, 10, 15, 20, 30, 40, and 50 Hz (10 cycles for each frequency) twice for each composite: low strain 7% and high strain 100%. In the third viscoelastic measurement the samples were firstly vulcanized in the rheometer at 160 °C temperature, then cooled down to 100 °C and tested at a constant frequency (10 Hz), while the strain amplitude was changing: 0.1%, 0.2%, 0.4%, 0.6%, 0.8%, 1%, 2%, 4%, 6%, 8%, 10%, 20%, 40%, 60%, 80%, and 90% (10 cycles for each strain). Differential scanning calorimetry (DSC) was performed in order to assess the glass transition temperature of the composites by means of DSC 214 Polyma device manufactured by Netzch (Selb, Germany). The samples were heated from −80 to 40 °C, with a heating rate of 20 °C/min under nitrogen atmosphere.

Mechanical properties of the vulcanizates were tested by Zwick/Roell 1435 testing machine—before and after ceramization, and Zwick/Roell hardness tester (Ulm, Germany)—before ceramization.

Combustibility of composite vulcanizates was determined by a cone calorimeter (Fire Testing Technology Ltd., East Grinstead, UK). Samples with dimensions of 100 mm × 100 mm × 2 mm were placed horizontally in relation to the IR heating source of 35 kW/m^2. The oxygen index test was performed on a home-made device in accordance with the ISO 4589-2:2017 standard [46]. Vertical fire spread test was performed in accordance to UL-94 standard [47]. Thermogravimetric analysis was done under synthetic air or nitrogen atmosphere with heating rate of 20 °C/min by means of Discovery TGA 550 device from TA Instruments (Crawley, UK)

Ceramization of the composite vulcanizates was performed in a laboratory furnace FCF 2.5SM (Czylok, Poland). Cylindrical samples (diameter–16 mm, height–8 mm) of the composites were heated in 3 different conditions: (1) 1100 °C—from room temperature to 1100 °C in 30 min (heating rate 35 °C/min); (2) 950 °C—from room temperature to 950 °C in 120 min (heating rate 7.5 °C/min); and (3) 550–1000 °C—from room temperature to 550 °C in 53 min (heating rate 10 °C/min), 10 min of isothermal conditions at 550 °C and at the end heating from 550 to 1000 °C in 27 min (heating rate 16 °C/min)—total time 90 min.

Micromorphology of the composites was examined before and after ceramization by means of scanning electron microscopy (SEM) Jeol JSM-6400 (JEOL Ltd., Tokyo, Japan) with Noran energy-dispersive X-ray spectroscope unit (EDS) (Thermo Fisher Scientific, Waltham, MA, USA). Sample cross sections were prepared by crushing in liquid nitrogen and gold sputtered directly before the measurements.

3. Results and Discussion

3.1. Viscoelastic Behavior and Vulcanization of Composites

The complex dynamic viscosity η* which is measured by an oscillating rheometer is analogous to the viscosity η_{app} measured by a capillary rheometer [48–51]. The complex dynamic viscosity η* is calculated from parameters obtained from rubber process analyzer (RPA) as follows:

The complex shear modulus (G^*) relation to storage shear modulus (G') and loss shear modulus (G'') is presented by the Equation (1):

$$G^* = \sqrt{(G')^2 + (G'')^2} \quad (1)$$

The complex dynamic viscosity (η*) relation to complex shear modulus (G^*) is given by Equation (2):

$$\eta^* = \frac{G^*}{\omega} \quad (2)$$

where ω—frequency (Hz).

Dynamic viscosity values both for low and high strain grew with the increasing quantity of mineral fillers (mica and fluxing agent). The addition of a fluxing agent had small impact even for low frequencies (Cyan_1 and Cyan_3; Figure 1 and Table 2). Mica used as filler with platelet-shape particles changed the viscosity of the composites to the highest extent. It is especially visible for the composite Cyan_5 where the general content of additives is the same as for the composite Cyan_6. For which 25 phr of mica and 25 phr of fluxing agent was exchanged to melamine cyanurate. However, the changes in the mix dynamic viscosity was almost two times (low strain) and three times (high strain) higher.

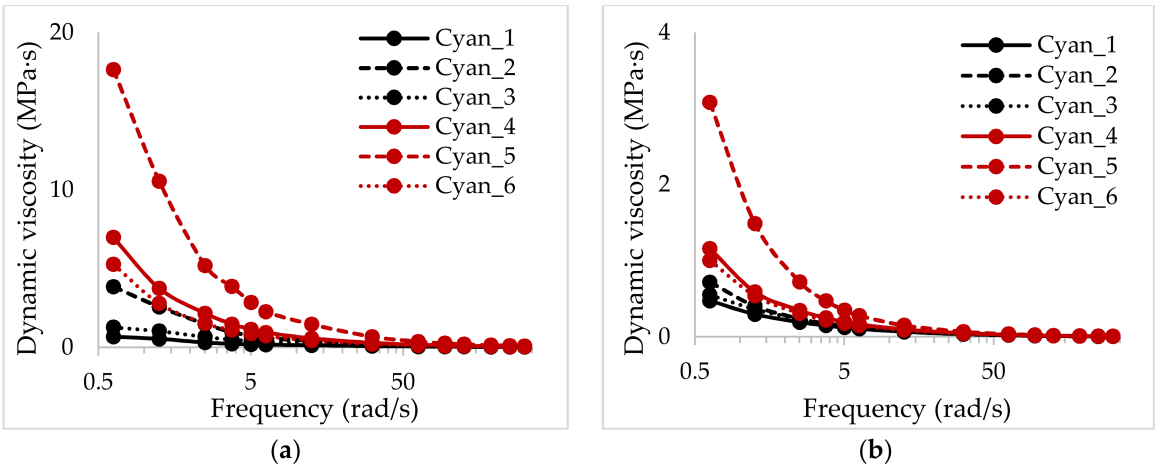

Figure 1. RPA dynamic complex viscosity versus frequency for the ceramizable composites: low strain 7% (**a**); and high strain 100% (**b**).

Table 2. Viscoelastic properties of uncured composites at chosen frequencies: storage shear modulus (*G′*), loss shear modulus (*G″*), and complex dynamic viscosity (η*).

Composite	Frequency (rad/s)	Low Strain (7%)			High Strain (100%)		
		G′ (kPa)	G″ (kPa)	η* (Pa·s)	G′ (kPa)	G″ (kPa)	η* (Pa·s)
Cyan_1	0.628	59.0	30.5	664373	33.2	33.7	473315
	5.024	110.5	88.8	177198	69.1	67.1	120421
	94.2	405.4	173.4	29392	160.3	129.8	13753
	314	555.8	185.9	11722	168.1	112.8	4048
Cyan_2	0.628	347.1	166.7	3851019	55.1	50.0	717635
	5.024	417.3	298.8	761623	78.5	79.8	139899
	94.2	1021.4	630.0	80004	143.9	140.3	13399
	314	1265.5	572.5	27779	144.8	125.1	3828
Cyan_3	0.628	129.8	41.7	1268917	33.8	43.5	550798
	5.024	243.4	215.8	406605	74.0	90.3	145999
	94.2	756.4	482.8	59822	170.5	170.8	160889
	314	1026.5	483.0	22690	173.8	149.3	4582
Cyan_4	0.628	566.6	407.1	6976724	75.7	87.9	1160105
	5.024	707.1	566.3	1132380	107.9	112.7	195047
	94.2	1376.9	885.3	109133	186.6	190.2	17763
	314	1657.0	872.5	37454	194.5	159.8	5035
Cyan_5	0.628	1586.0	772.2	17639995	199.7	234.4	3079313
	5.024	1777.1	1434.5	2854766	197.0	197.7	348841
	94.2	3142.7	2039.7	249772	251.9	253.6	23828
	314	3717.3	2014.6	84562	255.4	208.0	6588
Cyan_6	0.628	427.5	307.3	5264607	66.6	75.1	1003978
	5.024	560.5	402.0	862182	97.4	101.1	175427
	94.2	1072.9	674.5	84488	171.9	173.7	16294
	314	1271.1	672.9	29763	182.7	152.3	4758

What is surprising is the large difference between Cyan_4 and Cyan_5. The composition of both composites differed only by 25 phr of melamine cyanurate, and the dynamic viscosity changed from 7 to 18 MPa·s (low strain, 0.628 rad/s), and from 1 to 3 MPa·s (high strain, 0.628 rad/s). Given the insignificant/slight influence of MCA alone on mix viscosity (Cyan_1) it is clearly a synergistic effect between the mineral fillers and MCA. Probably this combination of the mineral fillers and melamine cyanurate results in a strong secondary structure formation, in which the mineral particles are connected with low-molecular MCA. It is clear that MCA itself is not able to form a secondary

structure in the SBR matrix (Figure 2). However, in the presence of additional mineral fillers it behaves like inter-particular low molecular binder resulting in a strong Payne effect. It is especially visible for composites Cyan_5 and Cyan_6. When the amount of fillers was reduced, the viscosity and G′ values dropped significantly. It is noticeable in the literature that application of low-molecular additives into rubber matrices may alter their viscoelastic properties to a significant extend [52].

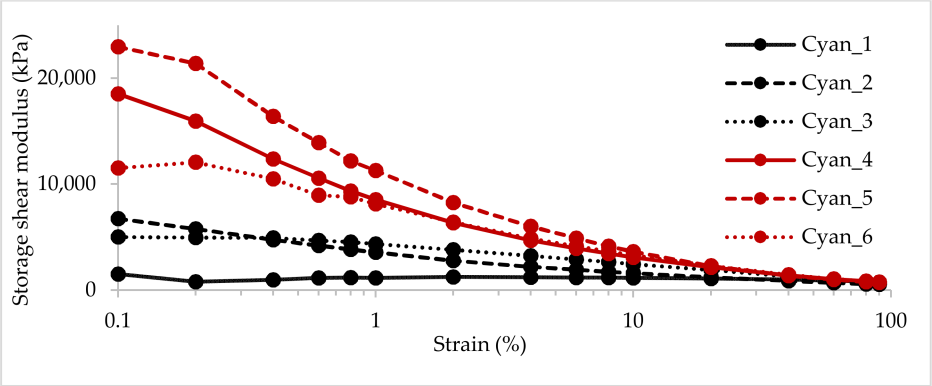

Figure 2. Strain amplitude dependence of storage shear modulus *G′* for cured ceramizable composites.

The viscosity of the mixes is a crucial factor during their processing, especially extrusion, which is commonly used for cable production. If the viscosity of rubber mixes is too high, their processing may be much more difficult or even impossible. Therefore, knowledge regarding the ability of a mica/glass frit/MCA system to form a strong secondary structure is of great importance.

The value of storage shear modulus *G′* as a function of growing strain shows how the secondary structure formed by fillers is destroyed, thus reducing the viscosity of the system. This effect is independent from a polymer matrix properties, but is caused by the specific filler–filler interactions, whose range is limited. Melamine cyanurate, both with mica and a fluxing agent, creates a structure with almost the same interactions (Figure 2). The highest values in dynamic viscosity for the Cyan_5 composite can be the result of the strongest interactions, which are created between filler particles connected by the low-molecular MCA. This can be explained by the chemical nature of the fillers—all three of them exhibit highly polar characteristics in opposition to the SBR matrix. Therefore, they are more likely to interact with each other resulting in a strong filler–filler secondary structure. In each case the addition of all three types of fillers causes stronger interactions than in the case when one of the fillers is not used.

The incorporation of fillers into the e-SBR rubber matrix resulted in a significant decrease of scorch time and optimum vulcanization time (Table 3 and Figure 3 and Figures S1–S6). The chemical structure of the melamine, containing three amine groups, indicates its possible vulcanization-acceleration feature. The application of only 50 phr of MCA resulted in a scorch time value of 5′ 30″. Surprisingly, the incorporation of additional mineral fillers (mica, glass frit) decreased this value very significantly. This is most probably the effect of a better distribution of MCA in the rubber matrix in the presence of additional mineral fillers. The incorporation of mineral fillers increases the shear forces during mixing resulting in better dispersion of MCA. Moreover, it is possible that some MCA molecules adsorb on the filler surface, which additionally enhances their dispersion and distribution in the e-SBR rubber matrix. This phenomenon may pose a threat on the processability of the composite mixes causing premature vulcanization. Increase in torque value stabilizes on a plateau for all composites showing no signs of reversion during the one hour of testing.

Table 3. Vulcanization parameters of the ceramizable composite mixes.

Vulcanization Parameter	Composite Mixes					
	Cyan_1	**Cyan_2**	**Cyan_3**	**Cyan_4**	**Cyan_5**	**Cyan_6**
Scorch time (t_{05})	5′ 30″	3′ 45″	2′ 0″	1′ 00″	2′ 15″	1′ 0″
Torque at t_{05} (dNm)	2.1	5.2	3.3	10.2	26.3	8.9
Optimum curing time (t_{90})	12′ 45″	9′ 0″	9′ 30″	6′ 45″	6′ 15″	6′ 30″
Torque at t_{90} (dNm)	15.8	24.0	26.5	41.8	57.2	37.9

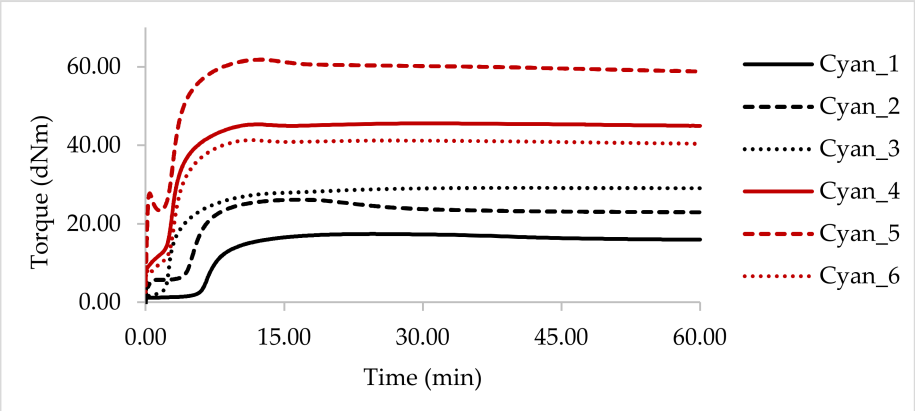

Figure 3. Vulcanization kinetics of composite mixes measured 24 h after preparation.

The addition of fillers does not influence the glass transition temperature (T_g), which fully depends on the SBR matrix (Figure 4). Composites' T_g values oscillate around –48 °C, which is equal to unfilled and uncured SBR given by its producer. Apparently large particles of mica, glass frit, and MCA do not interfere segmental macromolecular movement. This was expected because of particle size and their poor interfacial compatibility with the rubber matrix. All the fillers exhibit polar surface properties, whereas the rubber is highly non-polar. Therefore there is no factor that could constrain the segmental movement of the SBR macromolecules.

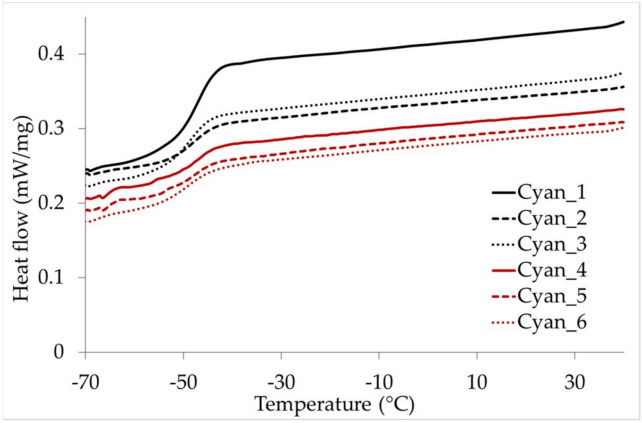

Figure 4. DSC curves of the composites.

3.2. Mechanical Properties of Composites before Ceramization

The effect of forming strong interactions between filler particles via MCA acting as a binder is also visible in mechanical properties of vulcanized composites (Table 4). For the composites, which were characterized by the three highest values of storage shear modulus G′, the elongation at break never reached 200%. Thus, composites elasticity was visibly reduced (except of Cyan_3) in comparison to the ceramizable composites we tested previously [36]. However, Cyan_5 which exhibits the highest

G' and tensile strength values shows higher E_b than Cyan_4 and Cyan_6. This is due to the most effective secondary structure formation by an optimal ratio of the incorporated fillers: 200/100/50 for mica/glass frit/MCA respectively. For Cyan_4 the amount of MCA is too low to act effectively as a low-molecular binder for the mica and glass frit. Whereas, for Cyan_6 the amount of the mineral fillers was too low with respect to MCA, which alone was not able to form a secondary reinforcing structure as shown by the Payne effect measurements (Figure 2). Therefore, the largest number of strongly connected filler particles was present in the Cyan_5 composite. Consequently, the value of Cyan_5 tear resistance reached 27.2 N/mm, which is the highest value for all the tested composites. The tensile strength of composites oscillated between 4.2 and 6.4 MPa, which is comparable to our previous results [36] and allows successful industrial applications.

Table 4. Mechanical properties of the vulcanizated composites: tear resistance (TES) stress at 100% (SE100), 200% (SE200), and 300% (SE300) of elongation, tensile strength (TS), elongation at break (E_b), and shore hardness, scale A and D.

Mechanical Parameter	Vulcanized Composites Description					
	Cyan_1	**Cyan_2**	**Cyan_3**	**Cyan_4**	**Cyan_5**	**Cyan_6**
TES (N/mm)	5.8 ± 0.5	22.7 ± 1.0	5.3 ± 0.4	12.9 ± 1.3	27.2 ± 3.2	14.2 ± 2.5
SE100 (MPa)	3.0 ± 0.2	4.7 ± 0.1	1.8 ± 0.1	4.4 ± 0.1	5.2 ± 0.2	4.5 ± 0.1
SE200 (MPa)	4.8 ± 0.4	5.5 ± 0.2	2.1 ± 0.1	–	–	–
SE300 (MPa)	–	–	3.1 ± 0.1	–	–	–
TS (MPa)	6.3 ± 1.3	6.3 ± 1.5	4.2 ± 0.5	4.8 ± 1.0	6.4 ± 0.5	4.7 ± 0.3
E_b (%)	248 ± 42	211 ± 33	345 ± 11	163 ± 9	188 ± 38	124 ± 34
Hardness (ShA)	60 ± 1	82 ± 1	71 ± 1	80 ± 1	81 ± 2	81 ± 1
Hardness (ShD)	11 ± 1	21 ± 1	14 ± 1	21 ± 1	21 ± 1	21 ± 1

The hardness of composites was most heavily impacted by the addition of mica. The addition of as little as 100 phr of other fillers to the composite, which already had 200 phr of mica did not affect its hardness, whereas the addition of fluxing agent affected the value of hardness but only when mica had not been already added. This is due to the fact that its stiff-platelet particulate structure increases the stiffness of composites significantly. In general, incorporation of fillers resulted in higher tensile strength and hardness of the composites, whereas elongation at break is reduced in comparison to the neat SBR vulcanizate [36].

3.3. Micromorphology of Composites before Ceramization

The micromorphology of samples investigated via SEM technique is presented in Figure 5.

Incorporation of fillers resulted in significant changes in the samples' micromorphology. The glass frit and mica were particular mineral fillers exhibiting high value of average particle size. Especially the glass frit particles, which often have a diameter >10 μm (Figure 5f), which influences negatively the mechanical and dynamic properties of rubbers. However, decreasing the size of glass frits is a challenging task due to their amorphous nature and low softening point temperature. They are prone to crushing as well as sintering in the same time during milling. Therefore, the smallest fraction of commercially available glass frits is often <63 μm. On the other hand, mica particles exhibit platelet structure of high aspect ratio (Figure 5d), whose incorporation results in formation of anisotropic, layered morphology during the vulcanization mixes in the pressurized mold (Figure 5c). This seems to be very beneficial from the point of view of fireproof performance of the coating by limiting heat and oxygen transfer into the bulk of the composite as well as flammable products of the rubber matrix degradation into the burning zone.

Due to highly polar nature of MCA its dispersion and distribution was very poor in a non-polar SBR matrix (Figure 5a). Furthermore, the wettability of the MCA agglomerates by the rubber macromolecules was very low (Figure 5b), and it was not improved by incorporation of the glass frit (Figure 5g). Even though the viscosity of the mixes increased after the addition of glass frit (Figure 1

and Table 2), the increase was not high enough to improve the dispersion and reduce the size of MCA agglomerates. On the other hand, adding mica platelets improved dispersion of MCA to a significant extent (Figure 5e). Firstly, because the presence of mica increased the viscosity to a much higher extent than the glass frit. Secondly, the mica particles are much finer and harder so they were able to defragment the MCA agglomerates resulting in a very homogenous distribution of MCA, which is confirmed by EDS nitrogen mapping (Figure 6a,e).

In general the microstructure of the composites was heterogeneous due to large size of the mineral filler (mica, glass frit) particles. However, adding mica resulted in very good MCA dispersion and distribution.

The composites containing all three fillers (Cyan_4, Cyan_5, and Cyan_6) exhibited very similar micromorphology (Figure 5h–m). Therefore, we decided to conduct EDS mapping on Cyan_5 sample as an example of elemental distribution (Figure 6).

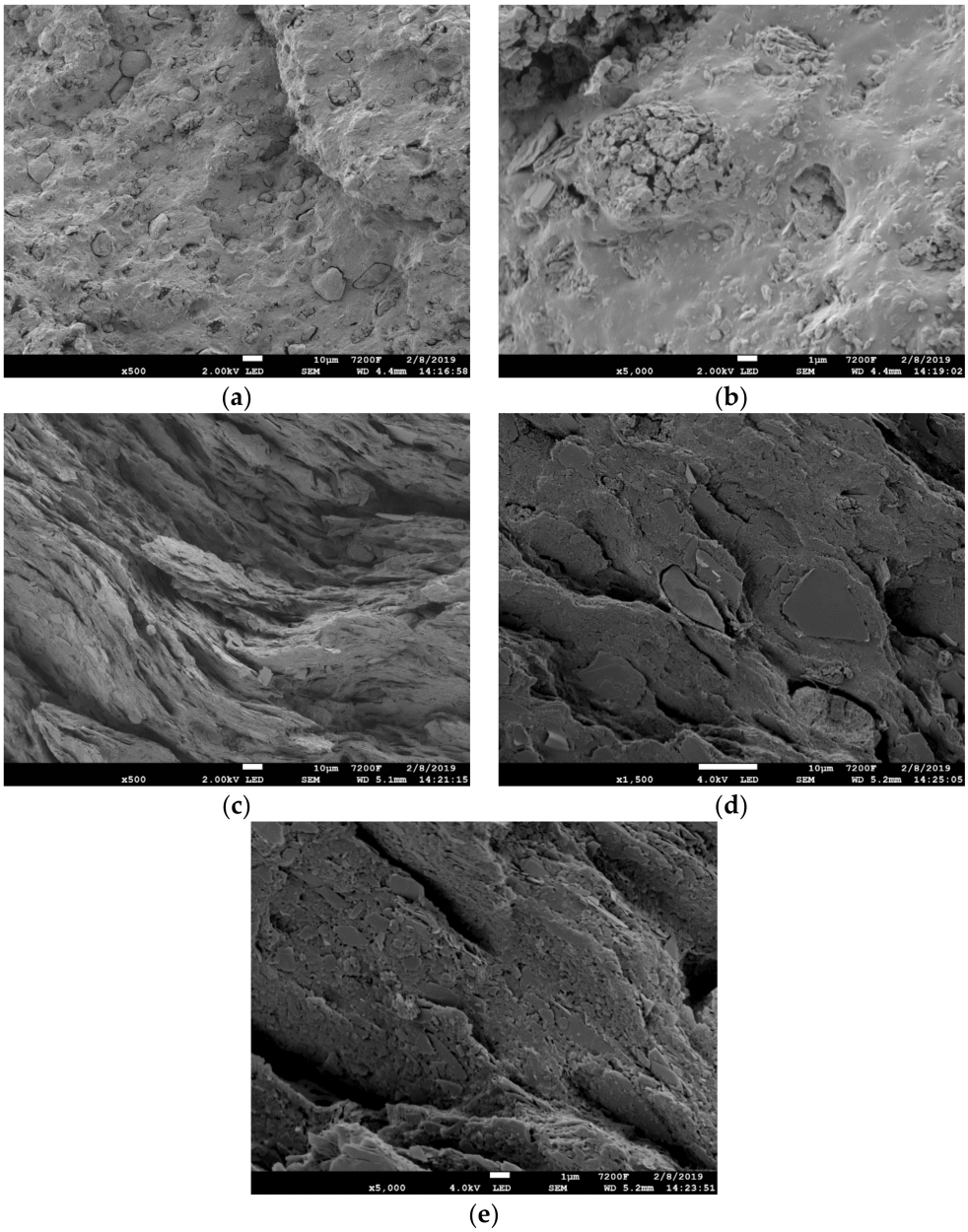

Figure 5. *Cont.*

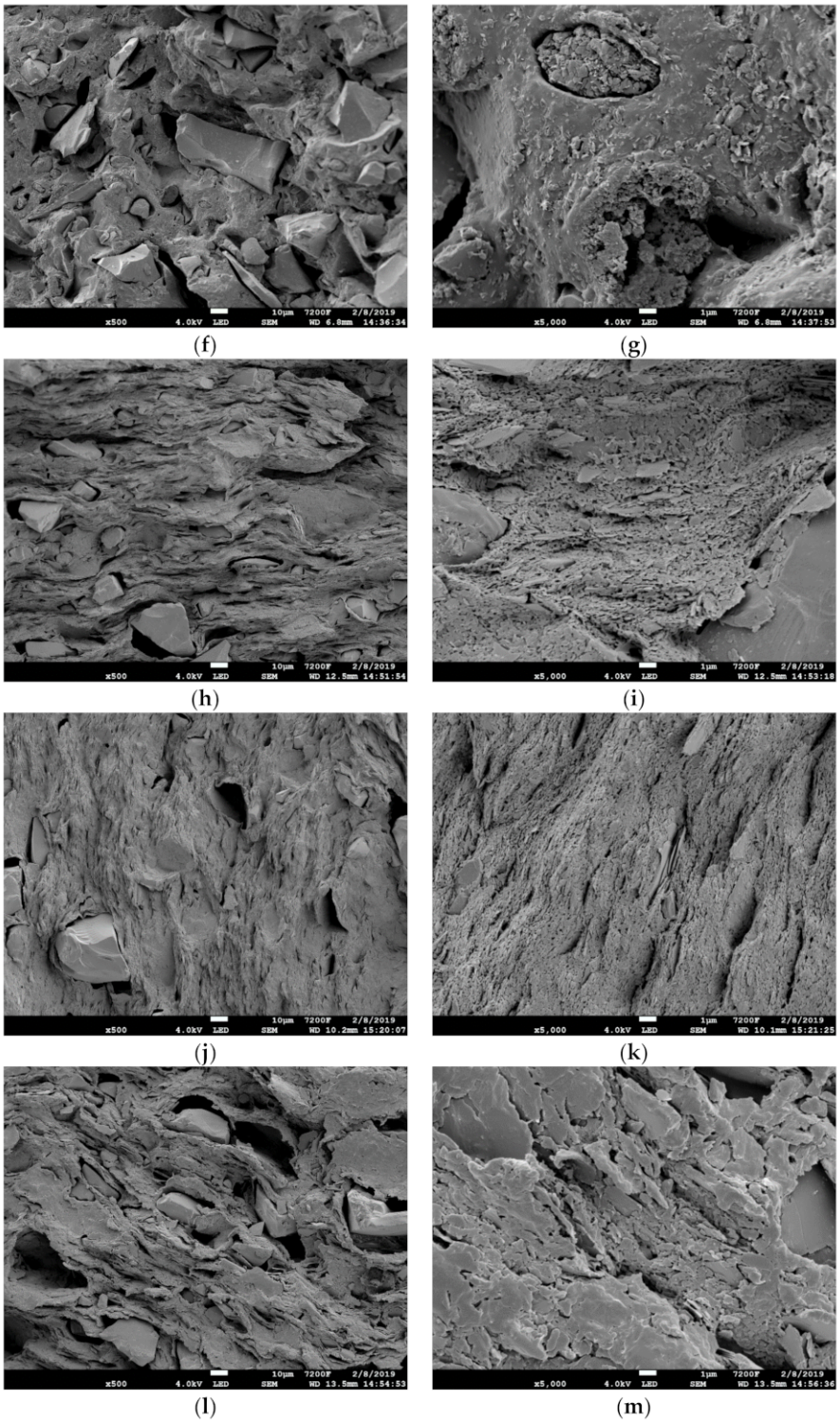

Figure 5. SEM photographs of composites' cross sections before ceramization: Cyan_1 with 500× (**a**) and 5000× (**b**) of magnification; Cyan_2 with 500× (**c**), 1500× (**d**), and 5000× (**e**) of magnification; Cyan_3 with 500× (**f**) and 5000× (**g**) of magnification; Cyan_4 with 500× (**h**) and 5000× (**i**) of magnification; Cyan_5 with 500× (**j**) and 5000× (**k**) of magnification; Cyan_6 with 500× (**l**) and 5000× (**m**) of magnification.

The glass frit applied consisted of a high quantity of silicon and sodium, and therefore its particles were easily detected by the EDS technique in the composite microstructure. EDS measurements confirmed results from the SEM analysis showing the composites' heterogeneous structure. Especially,

silicon (Figure 6h) and sodium (Figure 6f) maps indicated the position of glass frit particles. Nitrogen map (Figure 6e) confirmed good dispersion and distribution of MCA in the SBR matrix when mica was added. Magnesium (Figure 6d) and aluminum (Figure 6i) presence maps showed the location of mica particles indicating good dispersion and distribution of its particles in the composite.

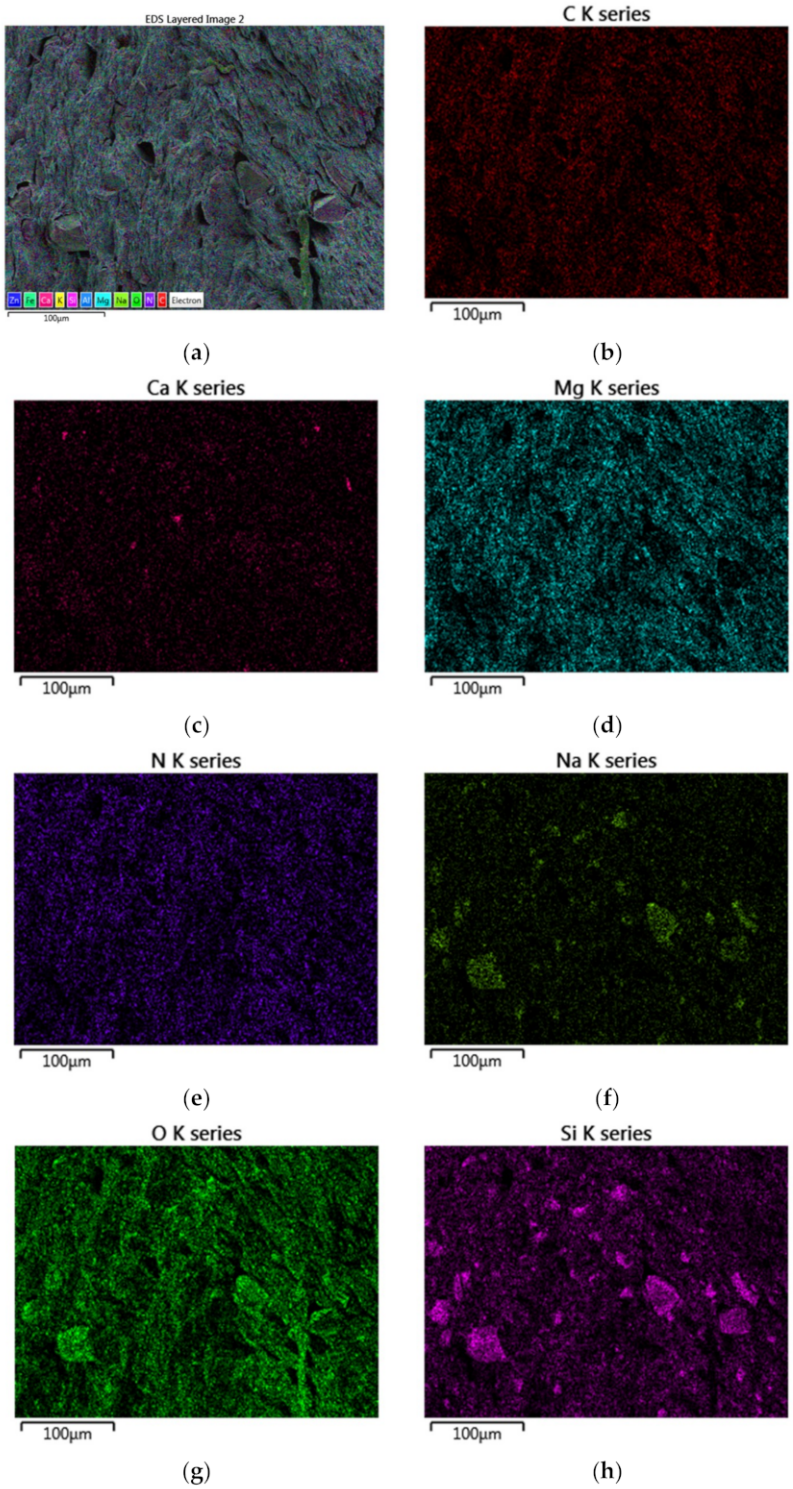

Figure 6. *Cont*.

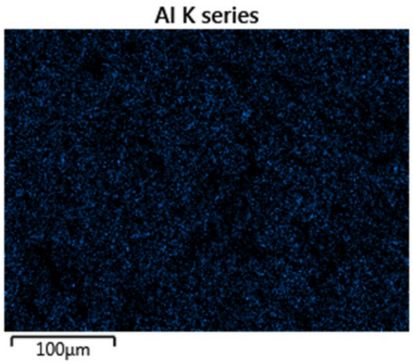

(**i**)

Figure 6. EDS mapping of Cyan_5 composite cross section before ceramization: summary map (**a**); carbon distribution (**b**); calcium distribution (**c**); magnesium distribution (**d**); nitrogen distribution (**e**); sodium distribution (**f**); oxygen distribution (**g**); silicon distribution (**h**); and aluminum distribution (**i**).

3.4. Flame Retardancy

The synergistic effect of ceramization and melamine cyanurate was visible especially in flammability properties of the tested composites (Figure 7 and Table 5). It was only the addition of mica or fluxing agent to the composition containing MCA that resulted in a decrease in THR from 50.2 to 16.1 or 38.6 mJ/m^2, respectively. For almost every combustibility parameter, the simultaneous effect of ceramization and melamine cyanurate was better than for each of them separately. Especially, the combination of MCA with mica resulted in significant improvement of flame retardancy of composites (Cyan_2) giving the lowest values of heat release rate, FIGRA (HRRp/tHRR ratio), and MAHRE (cumulative heat emission divided by time) parameters. This is due to the synergistic effect of carbonaceous char formation from MCA and large aspect ratio mica platelets, which can significantly improve the barrier properties of the char formed. This is most likely caused by the very homogenous dispersion and distribution of MCA in the presence of mica particles (Figure 5). Therefore, decreasing the transport of flammable hydrocarbon compounds formed from the thermal degradation of SBR rubber into the flame zone. Application of only glass frit with MCA did not improve fire resistance to a high extent, due to the fact that the frit does not promote effective ceramization alone and MCA dispersion is still poor. Time to ignition of the composites remained on the same level or increased from 89 to 222 s (Cyan_6), which was a significant improvement especially in comparison to the neat SBR vulcanizate [36]. Similarly, the flameout time exhibited very high values, which meant that the burning rate of the composites significantly decreased by the flame retardant performance of the mica/glass frit/MCA system. Mass loss decreased with the growing content of fillers that promote ceramization. The oxygen index value was very high in comparison to flame retarded SBR composites described in the recent literature [53,54], and reached 37.0% or 37.5% for the composites without mica, and exceeded 37.5% for composites with mica (37.5% is the limit value for the home-made apparatus on which the tests were carried out). The high combustibility parameter values of the studied composites placed them among other novel flame retardant systems for rubber application [55].

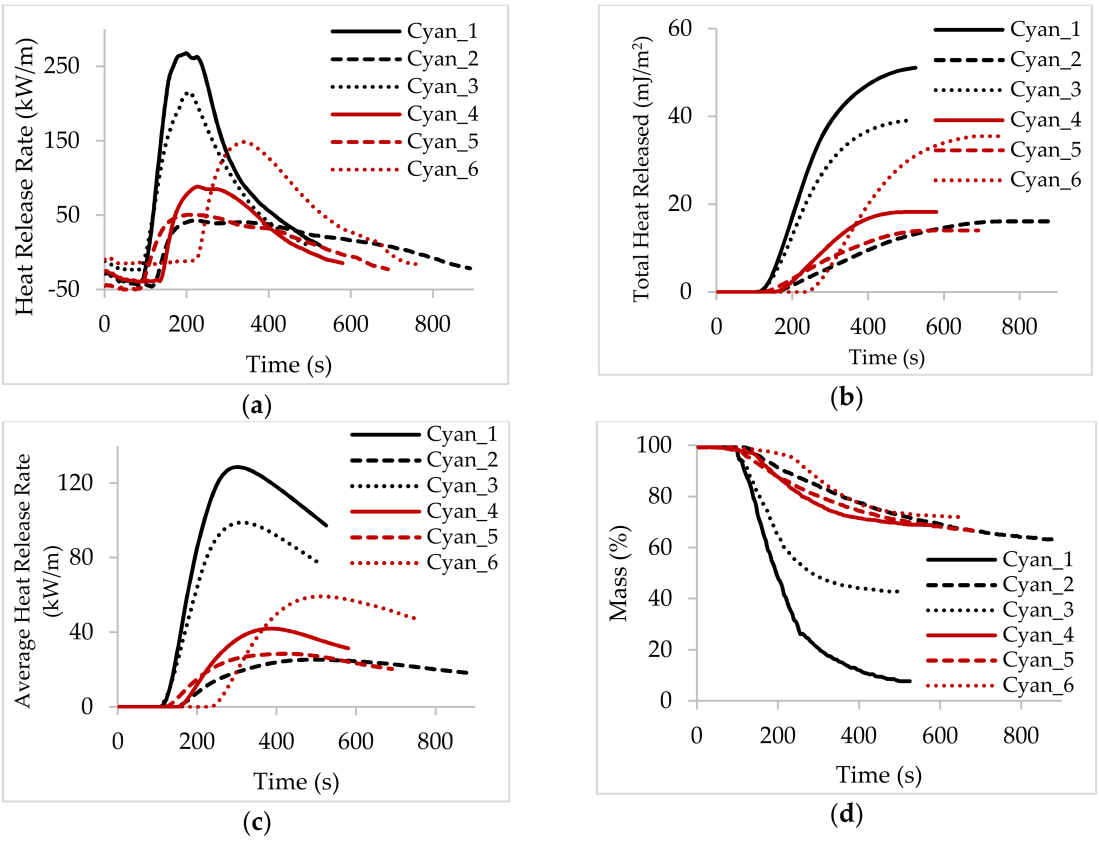

Figure 7. Cone calorimetry analysis of the composites: heat release rate (HRR) (**a**); total heat released (THR) (**b**); averaged heat release rate (ARHE) (**c**); and mass loss (**d**).

Table 5. Flammability parameters: time to ignition (t_i), time to flameout (t_o), heat release rate peak (HRR_p), heat release rate mean value (HRR_m), time to HRR_p (tHRR), HRR_p/tHRR ratio (FIGRA), total heat released (THR), effective heat of combustion peak (EHC_p), effective heat of combustion mean value (EHC_m), mass loss rate peak (MLR_p), mass loss rate mean value (MLR_m), cumulative heat emission divided by time (MARHE), mass loss (m_l), oxygen index (OI), and UL 94 fire test.

Combustibility Parameter	Vulcanized Composites Description					
	Cyan_1	Cyan_2	Cyan_3	Cyan_4	Cyan_5	Cyan_6
t_i (s)	89	119	93	134	86	222
t_o (s)	478	827	465	519	612	612
HRR_p (kW/m)	267.4	42.9	215.7	88.1	50.5	148.5
HRR_m (kW/m)	128.0	21.1	104.1	46.1	25.1	88.0
tHRR (s)	200	225	205	225	205	340
FIGRA (kW/ms)	1.34	0.19	1.05	0.39	0.24	0.43
THR (mJ/m^2)	50.2	16.1	38.6	18.2	14.0	34.2
EHC_p (mJ/kg)	76.6	59.2	79.0	50.3	26.4	72.0
EHC_m (mJ/kg)	20.7	8.5	20.4	12.6	8.0	24.1
MLR_p (g/s)	0.169	0.072	0.164	0.097	0.067	0.092
MLR_m (g/s)	0.055	0.022	0.045	0.032	0.028	0.032
MARHE (kW/m)	128	27	99	43	28	59
m_l (%)	91.3	35.6	56.6	28.8	31.7	24.9
OI (%)	37.0 ± 0.5	>37.5	37.5 ± 0.5	>37.5	>37.5	>37.5
UL 94	no rating	no rating	no rating	V-0	V-0	no rating
Burning droplets	no	no	no	no	no	no

For evaluating the flammability of the composites, the most important indicator is the FIGRA parameter value. This parameter is the value of Heat Release Rate peak divided by the time to reach this peak. Based on this parameter it is easy to compare the general flammability of composites, which depends not only on the heat generated during burning, but also on the time when this heat was emitted. The lower the value of this parameter the better fire resistance of a composite. Analyzing this parameter, the synergistic effect of ceramization and MCA-based char formation on flame retardancy of the composites were observed. For the composite containing only melamine cyanurate (Cyan_1), the value of this parameter was 1.34, the composite containing 200 phr of mica and 100 phr of fluxing agent—1.05. In each case, when melamine cyanurate and the full ceramization system were used, the value for this parameter was below 0.5: Cyan_4—0.39, Cyan_5—0.24, and Cyan_6—0.43. The presence of fluxing agent reduced the thermal properties (Cyan_2—0.19 compare to Cyan_3—1.05) but not to a high extent. Nevertheless, this filler is necessary for creating strong ceramic structures during ceramization, which will also work as thermal and mechanical stress barrier. The combustibility parameter values were significantly improved when MCA was applied to the ceramizable compositions in comparison to the e-SBR based composites we studied previously [36] that did not contain MCA.

3.5. Thermal Stability

Thermal stability of the composites under oxidative (synthetic air) or inert (nitrogen) atmospheres is presented in Figure 8 and Table 6.

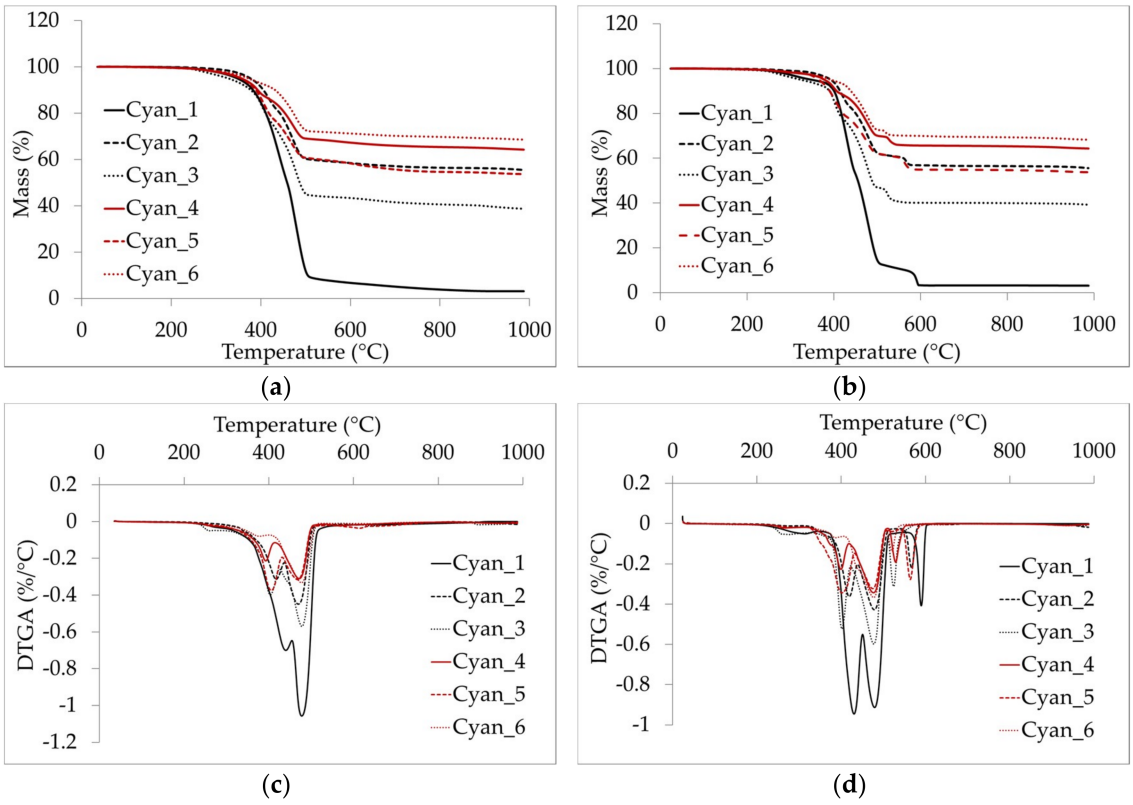

Figure 8. Thermogravometric analysis of the composites under nitrogen atmosphere: TGA (**a**) and DTGA (**c**); and under synthetic air atmosphere: TGA (**b**) and DTGA (**d**).

Table 6. Thermal stability parameters of the composites: temperature of 5% mass loss (T_5), maximum rate of first (DRT_{max1}), second (DRT_{max2}), and third (DRT_{max3}) step of degradation and their temperatures respectively (T_{max1}, T_{max2}, and T_{max3}), residue after thermal degradation.

Combustibility Parameter	Vulcanized Composites Description					
	Cyan_1	**Cyan_2**	**Cyan_3**	**Cyan_4**	**Cyan_5**	**Cyan_6**
Nitrogen Atmosphere						
T_5 (°C)	347.4	376.7	327.4	356.5	356.2	372.6
T_{max1} (°C)	438.8	416.7	405.8	385.2	403.6	379.4
DRT_{max1} (%/°C)	0.70	0.32	0.39	0.22	0.37	0.08
T_{max2} (°C)	479.6	470.1	479.9	469.1	467.8	478.8
DRT_{max2} (%/°C)	1.05	0.45	0.57	0.32	0.32	0.33
Residue (%)	3.1	55.5	38.7	64.2	53.7	68.6
Synthetic Air Atmosphere						
T_5 (°C)	349.3	393.4	324.5	378.5	365.8	393.7
T_{max1} (°C)	432.4	421.3	402.8	400.8	405.3	390.2
DRT_{max1} (%/°C)	0.94	0.36	0.52	0.22	0.34	0.07
T_{max2} (°C)	481.6	476.8	478.6	478.4	477.8	478.9
DRT_{max2} (%/°C)	0.91	0.43	0.60	0.34	0.32	0.36
T_{max3} (°C)	590.9	569.3	525.3	530.0	564.8	522.0
DRT_{max3} (%/°C)	0.40	0.22	0.31	0.19	0.28	0.14
Residue (%)	3.1	55.6	39.3	64.3	53.8	68.3

Addition of mica platelets improves thermal stability of the composites (Table 6). The beginning of thermal degradation temperature (T_5) reached the highest value for the composite filled with only mica and MCA (Cyan_2). This was most probably due to the layered structure of mica platelets and anisotropic morphology of the samples that reduce heat flow (mica platelets arranged in parallel can act as mirrors reflecting the infrared heat rays) into the bulk of composites and oxygen penetration. Glass frit decreases thermal stability most likely by increasing heat conductivity. Moreover, the spherical particles of the glass frit might cause formation of voids filled with air during mixing. This could increase the rate of in-bulk thermal oxidation of the SBR matrix.

The samples tested under nitrogen atmosphere exhibited double step thermal degradation kinetics (Figure 8c). This is most probably due to the different decomposition kinetics of SBR and MCA. After incorporating mineral fillers, the first step moves to lower temperatures (Table 6). This might be a result of a catalytic effect of the mineral fillers surface promoting the thermal decomposition of rubber. At the same time, the second step of the decomposition took place under similar temperatures for all composites, suggesting that it originated from MCA decomposition.

The kinetics changed with changes in the test atmosphere to oxidative synthetic air (Figure 8b,d). An extra third step of thermal decomposition appeared for the samples measured under synthetic air at higher range of temperatures. This is most likely a result of residual carbon char burning formed from MCA. This phenomenon is confirmed by the literature, in which the decomposition of MCA filled polymers under nitrogen proceeds without the final third step [56]. With the addition of mineral fillers, the temperature of the maximum decomposition of the third step of degradation shifted to lower temperatures. This is related to the amount of carbonized char formed during the thermooxidative decomposition: low—Cyan_3, Cyan_4 and Cyan_6 or high—Cyan_1, Cyan_2, and Cyan_5 (Figure 8b).

3.6. Properties of Composites after Ceramization

The composite containing only melamine cyanurate (Cyan_1) without fillers, which promote ceramization, in every case failed to create any ceramic structure, which was expected. The rest of the composites formed ceramic structures during heating but only the sample Cyan_3 did not change its shape much after ceramization to 1100 °C and could be tested for its compression strength.

The presence of both mica and fluxing agent was necessary to create a strong enough ceramic structure (Figure 9 and Table 7). The addition of mica (Cyan_2) or fluxing agent (Cyan_3) separately to the composite mix also resulted in a ceramic structure but with much worse compression strength properties. The application of melamine cyanurate along with mica and glass frit to the ceramizable compositions did not influence the mechanical properties of the composites after ceramization. In the composites with changing content of MCA (25–100 phr; Cyan_4–Cyan_6) the compression strength changed only within the limits of statistical error. Although it may seem that the error is very high, the samples' morphology after ceramization was far from homogenous in macro scale (Figure 10). Similar to random fire conditions, heating up relatively big samples containing many dispersed fillers results in their deformation due to several factors, such as: the initial inhomogeneity of their bulk structure; internal gas formation rate from degrading polymer matrix; carbonization of the polymer and MCA; thermal expansion of the mineral fillers; direction of the gas convection flow formed by the flame direction, etc.

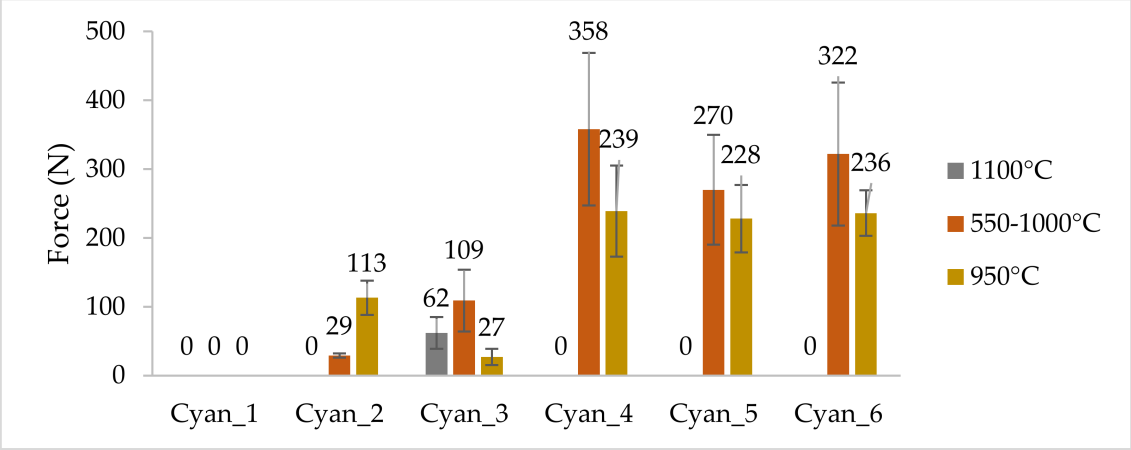

Figure 9. Compression strength of the ceramized composites studied.

Table 7. Compression strength of the ceramized composites studied.

Ceramization Conditions	Vulcanized Composites Description					
	Cyan_1	**Cyan_2**	**Cyan_3**	**Cyan_4**	**Cyan_5**	**Cyan_6**
1100 °C	–	–	62 ± 23	–	–	–
550–1000 °C	–	29 ± 3	109 ± 45	358 ± 111	270 ± 80	322 ± 104
950 °C	–	113 ± 25	27 ± 12	239 ± 66	228 ± 49	236 ± 33

The appearance of composites after ceramization (Figure 10) for those containing mica was almost the same. The Cyan_1 composite evaporated during the heat treatment. The composite in which the glass frit was not used (Cyan_2), had many visible cracks being marks of a relatively weak inter-particulate bonding. There was no binding material that was able to effectively connect particles of mica during heating. The composites Cyan_4–Cyan_6 looked almost the same, which was also mirrored in their compression strength. For these samples, a stiff, durable and porous ceramic structure was observed. The sample Cyan_3 differed from the other samples since the fluxing agent during heat treatment connected only to the polymer matrix decomposition products accompanied with MCA carbonization residues, which resulted in the black color of this sample. However, the fact that Cyan_3 could withstand the severe ceramization conditions with only the carbonaceous char formed from MCA, SBR, and glass frit shows a high potential of these ingredients for ceramizable composites manufacturing.

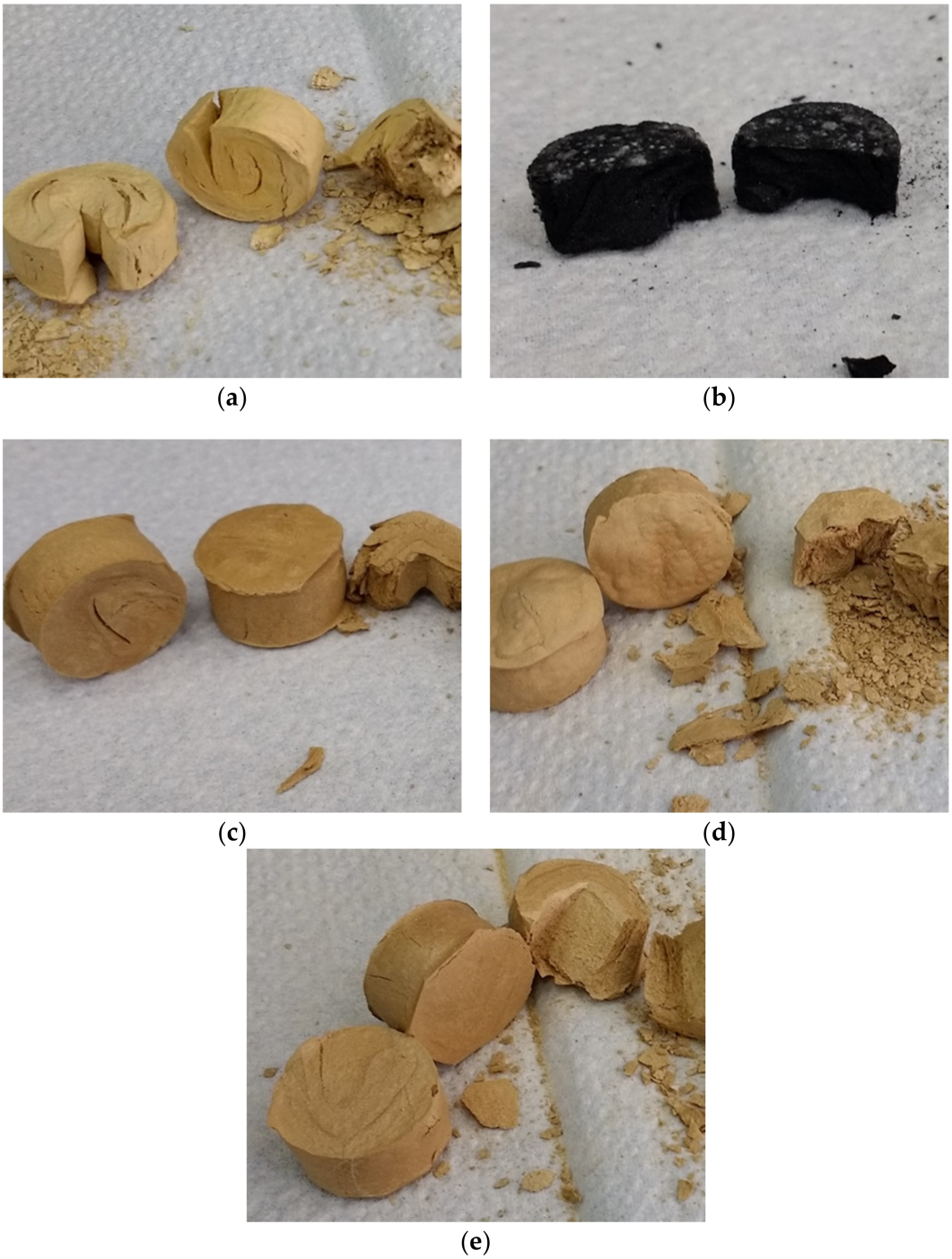

Figure 10. Appearance of composites after ceramization (950 °C) and the compression test: Cyan_2 (**a**); Cyan_3 (**b**); Cyan_4 (**c**); Cyan_5 (**d**); and Cyan_6 (**e**).

3.7. Micromorphology of Composites after Ceramization

In order to examine more in depth the effects of ceramization on the composites micromorphology, the Cyan_5 sample was chosen as an example. The mechanical properties of Cyan_4, Cyan_5, and Cyan_6 after ceramization were similar as was their micromorphology. Therefore, Cyan_5 should be a good example for the investigation (Figures 11 and 12).

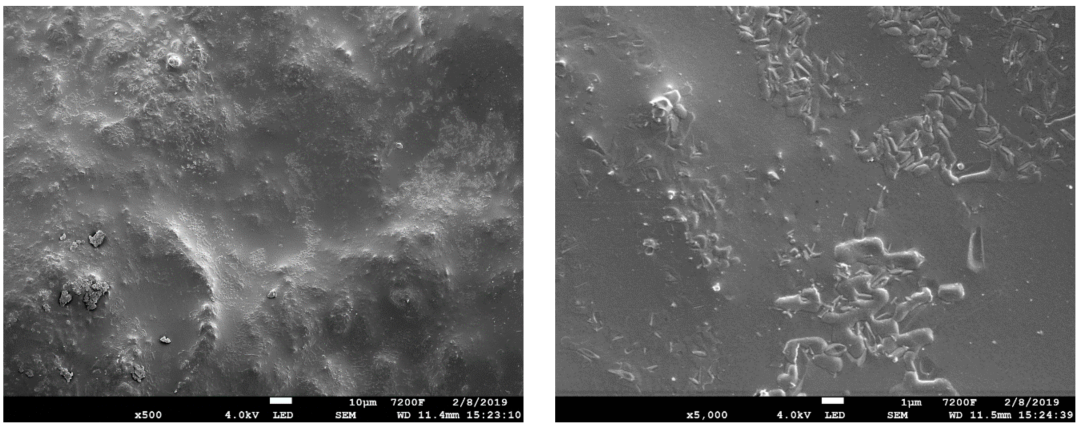

(**a**) (**b**)

Figure 11. SEM photographs of Cyan_5 composite cross section after ceramization with 500× (**a**) and 5000× (**b**) magnification.

SEM photographs of Cyan_5 sample ceramized in mild conditions (950 °C) revealed a solid and continuous microstructure (Figure 11) responsible for the good mechanical durability under compression test (Figure 9). However, the ceramic structure obtained was not homogenous on a micro scale level. Clear phase separation can be distinguished, especially under higher magnification (Figure 11b). This shows that the interphase adhesive forces are high resulting in good mechanical properties of the ceramic structure. For further phase analysis EDS mapping was performed (Figure 12).

EDS elemental mapping revealed the composition of the interphase structure (Figure 12a). Magnesium-rich islands clearly indicated (Figure 12b) the area where mica platelets are located on the surface of the sample's cross-section. High sodium concentration (Figure 12c) accompanied with the lack of magnesium and aluminum showed the area rich in softened glass frit in the upper part of the middle area of the photograph. Elemental analysis confirmed the non-homogeneity of the ceramic structure on a micro scale level. Regardless, high interfacial interactions between mica and glass frit resulted in high mechanical performance of the ceramized composite.

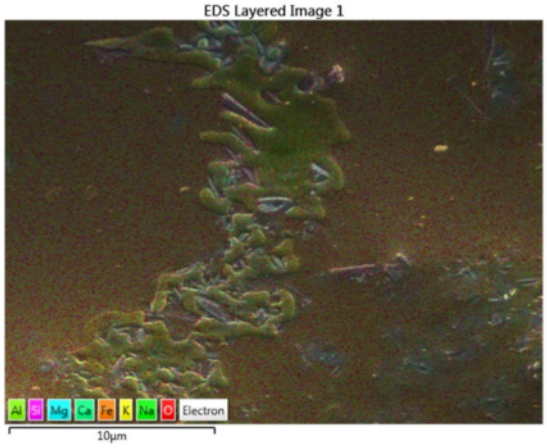

(**a**)

Figure 12. *Cont.*

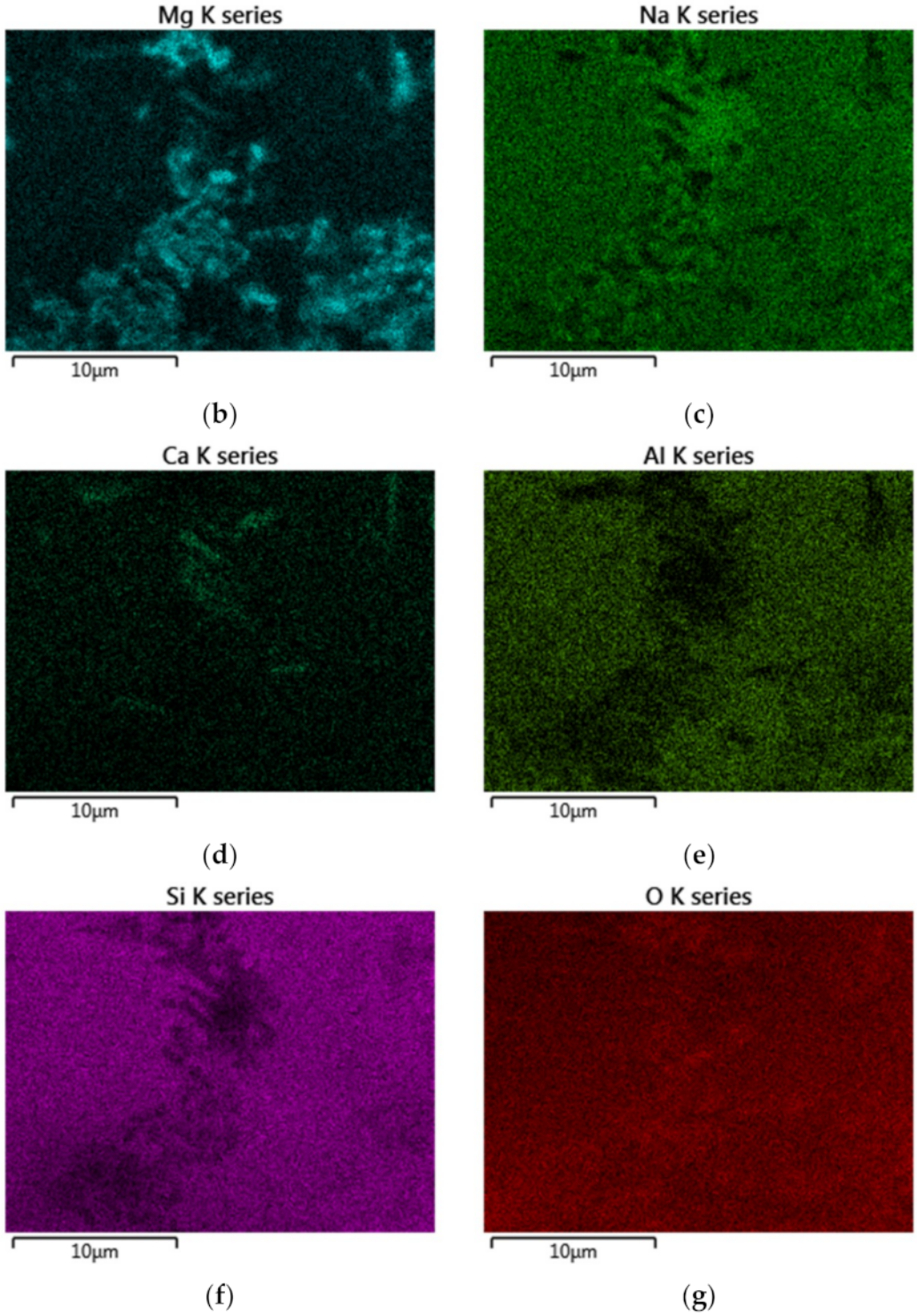

Figure 12. EDS mapping of Cyan_5 composite cross section after ceramization: summary map (**a**); magnesium distribution (**b**); sodium distribution (**c**); calcium distribution (**d**); aluminum distribution (**e**); silicon distribution (**f**); and oxygen distribution (**g**).

4. Conclusions

The addition of melamine cyanurate flame retardant improves flame retardant properties of ceramizable SBR-based composites. The synergistic effect is particularly visible for the fire resistance capacity of the composites measured by cone calorimetry, in which case, parameter improvement can reach six times better properties. Rheological properties of the mixes are also significantly affected by

the synergistic effect of mica/glass frit/MCA compositions. The mineral filler particles are connected by MCA particles acting as binders form a very strong secondary structure in the rubber matrix. However, this requires an optimum components ratio and can easily be changed by decreasing the amount of MCA or mineral fillers. SEM–EDS analysis showed that the micromorphology of the composites is heterogeneous. However, incorporation of mica platelets greatly improves MCA dispersion and distribution in the SBR matrix. Mechanical strength properties of the ceramizable composites vary in a significant range, however, the changes are not very significant from the real application point of view. The incorporation of different amounts of melamine cyanurate does not change compression strength of the composites after ceramization simultaneously increasing their fire resistance.

Supplementary Materials: The following are available online at http://www.mdpi.com/2079-6412/9/3/170/s1, Figures S1–S6: vulcanization kinetics of the Cyan_1–Cyan_6 composite mix (blue) and temperature of upper plate of the rheometer (orange) measured 24 h after preparation.

Author Contributions: Conceptualization, M.I., R.A. and D.M.B.; Investigation, M.I., R.A., M.L., P.R and B.S.; Resources, M.I.; Writing—Original Draft Preparation, M.I. and R.A.; Writing—Review and Editing, R.A.; Visualization, R.A.; Supervision, R.A. and D.M.B.; Project Administration, D.M.B.

Funding: This research received no external funding.

Acknowledgments: The authors would like to thank Xiaozhen He (Elastomer Technology and Engineering, Faculty of Engineering Technology, University of Twente) for support in TGA measurements, Nick Helthuis (Production Technology, Faculty of Engineering Technology, University of Twente) for SEM–EDS micromorphology photographs and Martyna Kościukiewicz for providing language help.

Conflicts of Interest: The authors declare no conflict of interest.

References

1. Hamdani, S.; Longuet, C.; Lopez-Cuesta, J.M.; Ganachaud, F. Calcium and aluminium-based fillers as flame-retardant additives in silicone matrices. I. Blend preparation and thermal properties. *Polym. Degrad. Stab.* **2010**, *95*, 1911–1919. [CrossRef]
2. Hamdani-Devarennes, S.; Pommier, A.; Longuet, C.; Lopez-Cuesta, J.M.; Ganachaud, F. Calcium and aluminium-based fillers as flame-retardant additives in silicone matrices II. Analyses on composite residues from an industrial-based pyrolysis test. *Polym. Degrad. Stab.* **2011**, *96*, 1562–1572. [CrossRef]
3. Hamdani-Devarennes, S.; Longuet, C.; Sonnier, R.; Ganachaud, F.; Lopez-Cuesta, J.M. Calcium and aluminum-based fillers as flame-retardant additives in silicone matrices. III. Investigations on fire reaction. *Polym. Degrad. Stab.* **2013**, *98*, 2021–2032. [CrossRef]
4. Liao, Y.J.; Liao, G.X.; Lo, S.M.; Ma, J.; Liu, S.B. A study on people's attitude to the use of elevators for fifire escape. *Fire Technol.* **2014**, *50*, 363–378. [CrossRef]
5. The Ultimate Passive Fire Protection Technology. Available online: http://www.cerampolymerik.com/downloads/cp-brochure-2006-03.pdf (accessed on 14 December 2018).
6. Gardelle, B.; Duquesne, S.; Vandereecken, P.; Bourbigot, S. Resistance to fire of silicone-based coatings: Fire protection of steel against cellulosic fire. *J. Fire Sci.* **2014**, *32*, 374–387. [CrossRef]
7. Zhang, G.; Wang, F.; Huang, Z.; Dai, J.; Shi, M. Improved ablation resistance of silicone rubber composites by introducing montmorillonite and silicon carbide whisker. *Materials* **2016**, *9*, 723. [CrossRef] [PubMed]
8. Luangtriratana, P.; Kandola, B.; Duquesne, S.; Bourbigot, S. Quantification of thermal barrier efficiency of intumescent coatings on glass fibre-reinforced epoxy composites. *Coatings* **2018**, *8*, 347. [CrossRef]
9. Anyszka, R.; Bieliński, D.M.; Pędzich, Z.; Parys, G.; Rybiński, P.; Zarzecka-Napierała, M.; Imiela, M.; Gozdek, T.; Siciński, M.; Okraska, M.; et al. Effect of mineral filler additives on flammability, processing and use of silicone-based ceramifiable composites. *Polym. Bull.* **2018**, *75*, 1731–1751. [CrossRef]
10. Lou, F.; Cheng, L.; Li, Q.; Wei, T.; Guan, X.; Guo, W. The combination of glass dust and glass fiber as fluxing agents for ceramifiable silicone rubber composites. *RSC Adv.* **2017**, *7*, 38805–38811. [CrossRef]
11. Wang, J.; Ji, C.; Yan, Y.; Zhao, D.; Shi, L. Mechanical and ceramifiable properties of silicone rubber filled with different inorganic fillers. *Polym. Degrad. Stab.* **2015**, *121*, 149–156. [CrossRef]

12. Xiong, Y.; Shen, Q.; Chen, F.; Luo, G.; Yu, K.; Zhang, L. High strength retention and dimensional stability of silicone/alumina composite panel under fire. *Fire Mater.* **2012**, *36*, 254–263. [CrossRef]
13. Delebecq, E.; Hamdani-Devarennes, S.; Raeke, J.; Lopez Cuesta, J.M.; Ganachaud, F. High residue contents indebted by platinum and silica synergistic action during the pyrolysis of silicone formulations. *ACS Appl. Mater. Int.* **2011**, *3*, 869–880. [CrossRef] [PubMed]
14. Hu, S.; Chen, F.; Li, J.G.; Shen, Q.; Huang, Z.X.; Zhang, L.M. The ceramifying process and mechanical properties of silicone rubber/ammonium polyphosphate/aluminium hydroxide/mica composites. *Polym. Degrad. Stab.* **2016**, *126*, 196–203. [CrossRef]
15. Zhang, X.; Guan, Y.; Xie, Y.; Qiu, D. "House-of-cards" structures in silicone rubber composites for superb anti-collapsing performance at medium high temperature. *RSC Adv.* **2016**, *6*, 7970–7976. [CrossRef]
16. Anyszka, R.; Bieliński, D.M.; Pędzich, Z.; Szumera, M. Influence of surface-modified montmorillonites on properties of silicone rubber-based ceramizable composites. *J. Therm. Anal. Calorim.* **2015**, *119*, 111–121. [CrossRef]
17. Imiela, M.; Anyszka, R.; Bieliński, D.M.; Pędzich, Z.; Zarzecka-Napierała, M.; Szumera, M. Effect of carbon fibers on thermal properties and mechanical strength of ceramizable composites based on silicone rubber. *J. Therm. Anal. Calorim.* **2016**, *124*, 197–203. [CrossRef]
18. Rybiński, P.; Syrek, B.; Bradło, D.; Żukowski, W.; Anyszka, R.; Imiela, M. Influence of cenospheric fillers on the thermal properties, ceramisation and flammability of nitrile rubber composites. *J. Compos. Mater.* **2018**, *52*, 2815–2827. [CrossRef]
19. Anyszka, R.; Bieliński, D.M.; Pędzich, Z.; Zarzecka-Napierała, M.; Imiela, M.; Rybiński, P. Processing and Properties of Fire Resistant EPDM Rubber-Based Ceramifiable Composites. *High Temp. Mater. Proc.* **2017**, *36*, 963–969. [CrossRef]
20. Zou, Z.; Qin, Y.; Liu, L.; Huang, Z. Effect of the flux on the fire-resistance properties of cerami-fiable EPDM rubber composites. *Adv. Compos. Lett.* **2018**, *27*, 89–95. [CrossRef]
21. Liu, L.; Qin, Y.; Song, J.; Zhang, G.; Huang, Z. Preparation and properties of ceramifiable ethylene propylene diene monomer rubber composites reinforced with chopped polyimide fibers. *Acta Mater. Compos. Sin.* **2017**, *34*, 2800–2809. (In Chinese)
22. Al-Hassany, Z.; Genovese, A.; Shanks, R.A. Fire-retardant and fire-barrier poly(vinyl acetate) composites for sealant application. *Express Polym. Lett.* **2010**, *4*, 79–93. [CrossRef]
23. Wong, S.; Shanks, R. Fire-retardant and fire-barrier polyurethane foam sealants containing a ceramifying filler composition for structural integrity. In Proceedings of the 7th Asian-Australian Conference on Composite Materials, Taipei, Taiwan, 15–18 November 2010.
24. Shanks, R.A.; Wong, S.; Preston, C.M. Ceramifying fire-retardant and fire-barrier unsaturated polyester composites. *Adv. Mater. Res.* **2010**, *123*, 23–26. [CrossRef]
25. Wang, T.; Shao, H.; Zhang, Q. Ceramifying fire-resistant polyethylene composites. *Adv. Compos. Lett.* **2010**, *19*, 175–179.
26. Wang, F.; Huang, Z.; Liu, Y.; Li, Y. Novel cardanol-containing boron-modified phenolic resin composites: Non-isothermal curing kinetics, thermal properties, and ablation mechanism. *High Perform. Polym.* **2017**, *29*, 279–288. [CrossRef]
27. Shi, M.; Chen, X.; Fan, S.; Shen, S.; Liu, T.; Huang, Z. Fluxing agents on ceramification of composites of MgO–Al_2O_3–SiO_2/boron phenolic resin. *J. Wuhan Univ. Technol.* **2018**, *33*, 381–388. [CrossRef]
28. Fan, S.; Shi, M.; Meng, P.; Chen, X.; Huang, Z. Effects of fusing agent on the thermal behavior and microstructure of ceramifiable boron phenolic resin composites. *Acta Mater. Compos. Sin.* **2017**, *34*, 60–66. (In Chinese)
29. Di, H.W.; Deng, C.; Li, R.M.; Dong, L.P.; Wang, Y.Z. A novel EVA composite with simultaneous flame retardation and ceramifiable capacity. *RSC Adv.* **2015**, *5*, 51248–51257. [CrossRef]
30. Gong, X.; Wang, T. Optimisation of the ceramic-like body for ceramifiable EVA-based composites. *Sci. Eng. Compos. Mater.* **2017**, *24*, 599–607. [CrossRef]
31. Li, Y.M.; Deng, C.; Long, J.W.; Huang, S.C.; Zhao, Z.Y.; Wang, Y.Z. Improving fire retardancy of ceramifiable polyolefin system via a hybrid of zinc borate@melamine cyanurate. *Polym. Degrad. Stab.* **2018**, *153*, 325–332. [CrossRef]
32. Zhao, D.; Shen, Y.; Wang, T. Ceramifiable EVA/APP/SGF composites for improved ceramifiable properties. *Polym. Degrad. Stab.* **2018**, *150*, 140–147. [CrossRef]

33. Ferg, E.E.; Hlangothi, S.P.; Bambalaza, S. An experimental design approach in formulating a ceramifiable EVA/PDMS composite coating for electric cable insulation. *Polym. Compos.* **2017**, *38*, 371–380. [CrossRef]
34. Song, J.Q.; Huang, Z.X.; Qin, Y.; Yang, G.Y.; Wang, X. Ceramifiable and mechanical properties of silicone rubber foam composite with frit and high silica glass fiber. *IOP Conf Ser-Mat. Sci.* **2018**, *423*, 012168. [CrossRef]
35. Guo, J.; Chen, X.; Zhang, Y. Improving the mechanical and electrical properties of ceramizable silicone rubber/halloysite composites and their ceramic residues by incorporation of different borates. *Polymers* **2018**, *10*, 388. [CrossRef]
36. Anyszka, R.; Bieliński, D.M.; Pędzich, Z.; Rybiński, P.; Imiela, M.; Siciński, M.; Zarzecka-Napierała, M.; Gozdek, T.; Rutkowski, P. Thermal Stability and Flammability of Styrene-Butadiene Rubber-Based (SBR) Ceramifiable Composites. *Materials* **2016**, *9*, 604. [CrossRef] [PubMed]
37. Amraee, I.A.; Katbab, A.A.; Aghafarajollah, S.H. Qualitative and quantitative analysis of SBR/BR blends by thermogravimetric analysis. *Rubber Chem. Technol.* **1996**, *69*, 130–136. [CrossRef]
38. Chen, K.S.; Yeh, R.Z.; Chang, Y.R. Kinetics of thermal decomposition of styrene-butadiene rubber at low heating rates in nitrogen and oxygen. *Combust. Flame* **1997**, *108*, 408–418. [CrossRef]
39. Varkey, J.T.; Augustine, S.; Thomas, S. Thermal degradation of natural rubber/styrene butadiene rubber latex blends by thermogravimetric method. *Polym. Plast. Technol. Eng.* **2000**, *39*, 415–435. [CrossRef]
40. Camino, G.; Lomakin, S.M.; Lazzari, M. Polydimethylsiloxane thermal degradation Part 1. Kinetic aspects. *Polymer* **2001**, *42*, 2395–2409. [CrossRef]
41. Camino, G.; Lomakin, S.M.; Lageard, M. Thermal polydimethylsiloxane degradation. Part 2. The degradation mechanisms. *Polymer* **2002**, *43*, 2011–2015. [CrossRef]
42. Rybiński, P.; Janowska, G. Influence synergetic effect of halloysite nanotubes and halogen-free flame-retardants on properties nitrile rubber composites. *Thermochim. Acta* **2013**, *557*, 24–30. [CrossRef]
43. Kmiotek, M.; Bieliński, D.M.; Anyszka, R.; Kleczewska, J.; Siciński, M. Flammability and thermal stability of vulcanized rubber mixes. *Przem. Chem.* **2013**, *92*, 1741–1746.
44. *ISO 37:1994 Rubber, Vulcanized or Thermoplastic–Determination of Tensile Stress-Strain Properties*; ISO: Geneva, Switzerland, 1994.
45. *ASTM D6204 Standard Test Method for Rubber—Measurement of Unvulcanized Rheological Properties Using Rotorless Shear Rheometers*; ASTM International: West Conshohocken, PA, USA, 2015.
46. *ISO 4589-2:2017 Plastics-Determination of Burning Behaviour by Oxygen Index-Part 2: Ambient-Temperature Test*; ISO: Geneva, Switzerland, 2017.
47. *UL 94 Standard for Tests for Flammability of Plastic Materials for Parts in Devices and Appliances*; UL: Bentonville, AR, USA, 2013.
48. Dick, J.S. Compound processing characteristics and testing. In *Rubber Technology Compounding and Testing for Performance*; Dick, J.S., Ed.; Hanser Publishers: Münich, Germany, 2001; pp. 17–43.
49. Gao, T.; Xie, R.; Zhang, L.; Gui, H.; Huang, M. Use of Rubber Process Analyzer for Characterizing the Molecular Weight Parameters of Natural Rubber. *Int. J. Polym. Sci.* **2015**, 517260. [CrossRef]
50. Dasgupta, S.; Agrawal, S.L.; Bandyopadhyay, S.; Mukhopadhyay, R.; Malkani, R.K.; Ameta, S.C. Improved polymer-filler interaction with an ecofriendly processing aid. Part 1. *Prog. Rubber Plast. Recycl. Technol.* **2009**, *25*, 141–164. [CrossRef]
51. Perko, L.; Friesenbichler, W.; Obendrauf, W.; Buchebner, V.; Chaloupka, G. Elongational viscosity of rubber compounds and improving corresponding models. *Adv. Prod. Eng. Manag.* **2013**, *8*, 126–133. [CrossRef]
52. Lipińska, M.; Imiela, M. Viscoelastic properties and curing of polyhedral oligomeric silsesquioxanes POSS modified ethylene-propylene hydrogenated nitrile rubber EPM/HNBR composites. *J. Multidiscip. Eng. Sci. Technol.* **2017**, *4*, 8544–8555.
53. Sung, K.I.; Lee, W.-K.; Park, C.Y. Fire resistant properties of SBR nanocomposites reinforced with flame retardants/montmorillonite. *Polymer* **2017**, *41*, 267–275. [CrossRef]
54. Wang, Z.; Kong, Q. Synthesis of a chitosan-based intumescent flame retardant and its application in SBR rubber. *Polym. Mater. Sci. Eng.* **2013**, *29*, 29–32.

55. Rybiński, P.; Syrek, B.; Bradło, D.; Żukowski, W. Effect of POSS particles and synergism action of POSS and poly(melamine phosphate) on the thermal properties and flame retardance of silicone rubber composites. *Materials* **2018**, *11*, 1298. [CrossRef] [PubMed]
56. Jiang, M.; Yu, Y.; Chen, Z. Environmentally friendly flame retardant systems for unsaturated polyester resin. *IOP Conf. Ser. Earth Environ. Sci.* **2018**, *170*, 032116. [CrossRef]

© 2019 by the authors. Licensee MDPI, Basel, Switzerland. This article is an open access article distributed under the terms and conditions of the Creative Commons Attribution (CC BY) license (http://creativecommons.org/licenses/by/4.0/).